SPAWAR
Systems Center
San Diego

DIMENSIONS
TECHNICAL REPORT 2

A Joint Maximum-Likelihood-Based Phase and Timing Synchronizer for Dual-*h*, Full-Response 4-ary CPM

R. H. Pettit
California State University, Northridge

B. E. Wahlen
SSC San Diego

SSC San Diego

Technical Document 3143
September 2002

A Joint Maximum-Likelihood-Based Phase and Timing Synchronizer for Dual-*h*, Full-Response 4-ary CPM

R. H. Pettit
California State University, Northridge

B. E. Wahlen
SSC San Diego

SSC San Diego
San Diego, CA 92152-5001

SSC SAN DIEGO
San Diego, California 92152-5001

T. V. Flynn, CAPT, USN
Commanding Officer

R. C. Kolb
Executive Director

ADMINISTRATIVE INFORMATION

The work described in this report was performed for the Office of Naval Research by the SSC San Diego Littoral Communications Systems Branch (Code 2846).

Released by
G. A. Garcia, Head
Littoral Communications
Systems Branch

Under authority of
D. Milstead, Head
RF Communications
Systems Division

SB

EXECUTIVE SUMMARY

Maximum-likelihood (ML) techniques are useful in finding synchronizer structures for various cases. Synchronizers for frequency, phase, and timing have been found for various bandpass signaling techniques such as PSK, DPSK, QAM, MSK, and CPM. These include data-aided, decision-directed, and clock-aided cases. This report describes a new non-data-aided, non-decision-directed ML-based phase and timing synchronizer for a dual-h, full-response, 4-ary CPM waveform. The derived structure will be incorporated into future simulations to compare performance among several possible phase and timing synchronizers.

This Page Intentionaly
Left Blank

CONTENTS

LIST OF FIGURES

LIST OF TABLES

I. INTRODUCTION

Successful operation of digital communication systems requires that receivers achieve synchronization. Carrier frequency and phase, waveform time-of-arrival, frame synchronization for time-division multiplexing (TDM)/time-division multiple access (TDMA), and timing for a frequency-hopping pattern or for a direct sequence spreading code for spread-spectrum are examples of typical unknowns that must be estimated for good performance.

There are many successful synchronization schemes. Mengali and D'Andrea [1] present theoretical and practical details for synchronizers of frequency, phase, and symbol timing for various baseband and bandpass signaling techniques, including phase-shift keying (PSK), differential phase-shift keying (DPSK), quadrature amplitude modulation (QAM), minimum-shift keying (MSK), and continuous-phase modulation (CPM). This paper generalizes their joint phase and timing synchronizer results for CPM with a single modulation index (single-h CPM) to CPM with two modulation indices (dual-h CPM), assuming a full-response, rectangular, instantaneous frequency pulse (1REC) and a 4-ary signaling alphabet [2]. In addition to frequency, phase, and symbol timing, the dual-h case also requires the so-called *super-baud* synchronization inherent with CPM using more than one modulation index. A previous report by Pettit and Wahlen [3] presented a frequency synchronizer for the same case.

Synchronizers are developed using either an ad hoc approach, based upon intuitive reasoning, or a formal approach, based upon techniques of estimation theory. Both approaches have proven useful and, in many cases, the ad hoc synchronizers fit within an estimation theory framework. We follow the formal approach, deriving a structure for joint phase and timing acquisition and tracking based upon the well-known *maximum likelihood (ML)* criterion of optimality (see [4], for example) which maximizes a probability density function for received samples conditioned upon a set of parameters to be estimated. We emphasize, however, that because of necessary approximations for analytical completion and receiver implementation, our final phase and timing recovery scheme is an approximation to the ML solution and is, therefore, suboptimal.

Final questions involving performance of this suboptimal synchronizer will require simulation methods because of inherent analytical complexities. A direct measure of the "goodness" of an estimator is its variance, usually compared to either the Cramer-Rao or the Modified Cramer-Rao lower bounds (see [1]). Ultimately, desirable performance would be in terms of effects on ability to correctly receive data when using the particular synchronization method. A future paper will present results from appropriate simulation studies.

This Page Intentionaly
Left Blank

II. General Structure for the Phase and Timing Synchronizer

The task is to find a phase and timing recovery scheme (acquisition and tracking) that can operate with random data and known frequency. Furthermore, the synchronizer is to be *non-data aided*, operating without benefit of a known data sequence such as a preamble, and *non-decision directed*, operating without benefit of a detected data sequence. The notation and modeling given below closely follow Mengali and D'Andrea [1] for single-h CPM, including complex envelope notation.

We assume that the *received waveform*, $r(t)$, is given by

$$r(t) = s(t) + w(t), \tag{1}$$

where

$$s(t) = e^{j\theta}\sqrt{\frac{2E_s}{T}}e^{j\psi(t\ \ \tau,\boldsymbol{\alpha})} \tag{2}$$

is the *CPM signal* and $w(t)$ is an additive *white Gaussian noise* component with spectral density, N_0. In equation (2), θ and τ represent the unknown *carrier phase* and *time-of-arrival*, respectively; E_s is the *signal energy* over the *symbol interval*, T; and $\boldsymbol{\alpha} = (\ldots, \alpha_{-1}, \alpha_0, \alpha_1, \ldots)$ is the *data sequence* with $\alpha_i \in \{\pm 1, \pm 3\}$ for the 4-ary case of interest. Note that there is no carrier frequency offset since carrier frequency is assumed to be known.

The *phase*, $\psi(t, \boldsymbol{\alpha})$, is given by

$$\psi(t, \boldsymbol{\alpha}) = 2\pi \sum_i \alpha_i h_{\underline{i}} q(t \quad iT)\ , \tag{3}$$

where $h_{\underline{i}}$ is the *modulation index* for the i^{th} interval and $q(t)$ is the *phase response* function. For the dual-h case, $h_{\underline{i}} = h_0$ is applied to $\boldsymbol{\alpha}_0 = (\ldots, \alpha\ _2, \alpha_0, \alpha_2, \ldots)$ while $h_{\underline{i}} = h_1$ is applied to $\boldsymbol{\alpha}_1 = (\ldots, \alpha\ _3, \alpha\ _1, \alpha_1, \alpha_3, \ldots)$. Thus,

$$\begin{aligned} \psi(t, \boldsymbol{\alpha}) &= 2\pi h_0 \sum_i \alpha_{2i} q(t - 2iT) + 2\pi h_1 \sum_i \alpha_{2i+1} q(t \quad [2i+1]T) \\ &\triangleq \psi_0(t, \boldsymbol{\alpha}_0) + \psi_1(t, \boldsymbol{\alpha}_1)\ . \end{aligned} \tag{4}$$

For the full-response, rectangular frequency pulse case (so-called 1REC), the phase response is a *ramp* function given by

$$q(t) = \begin{cases} 0, & \text{if } t < 0 \\ t/2T, & \text{if } 0 \le t \le T \\ 1/2, & \text{if } t > T. \end{cases} \tag{5}$$

In keeping with modern practice, we assume a *digital* synchronizer that processes discrete-time samples of the waveforms rather than an *analog* synchronizer that processes directly the continuous-time waveforms. The *samples*, $\boldsymbol{x} = \{x(kT_s)\}$, are taken as shown below (Figure 1) from the output of an *anti-aliasing filter (AAF)*, which is assumed to have sufficiently wide passband to pass the signal, $s(t)$, without significant distortion. Also, it is assumed that the *sampling period*, T_s, is sufficiently short to allow the samples to retain the information content of the continuous-time waveforms.

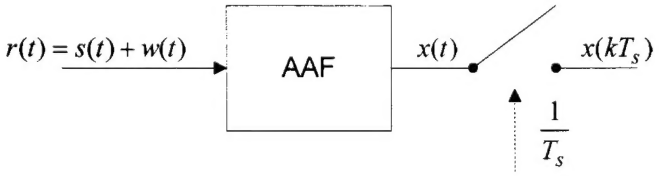

Fig. 1. Sampling output of anti-aliasing filter (AAF).

Additionally, we let L_0 be the *number of information symbols to be "observed"* for purposes of collecting the samples (L_0 is assumed to be an even integer), and let N be the *number of samples taken per symbol*. (Mengali and

D'Andrea suggest $N = 4$ as an appropriate value for cases studied by them.) Thus,

$$\begin{aligned} T_0 &= \text{"observation time"} \\ &= L_0 T \\ &= N L_0 T_s \end{aligned} \tag{6}$$

and

$$\boldsymbol{x} = \{x(0), x(T_s), \cdots, x([NL_0 - 1]T_s)\}. \tag{7}$$

The task is to derive a maximum-likelihood-based estimator of the unknown phase and timing which does not require knowledge of $\boldsymbol{\alpha}$. Hence, the *likelihood function*, $\Lambda(\boldsymbol{x}|\widetilde{\theta}, \widetilde{\tau})$, is obtained from the *conditional likelihood function*, $\Lambda(\boldsymbol{x}|\widetilde{\boldsymbol{\alpha}}, \widetilde{\theta}, \widetilde{\tau})$, by averaging over $\widetilde{\boldsymbol{\alpha}}$ as described in Mengali and D'Andrea [1]. Clarifying previously introduced and additional notation, we let

$$\begin{aligned} \theta &= \text{the } \textit{actual}\text{, but unknown, } \textit{phase}, \\ \widetilde{\theta} &= \text{a } \textit{possible value}\text{ of } \theta \text{ (a "realization")}, \\ \widehat{\theta} &= \text{an } \textit{estimate}\text{ of } \theta, \end{aligned}$$

and similarly for τ, $\widetilde{\tau}$, and $\widehat{\tau}$.

The conditional likelihood function is given by

$$\Lambda(\boldsymbol{x}|\widetilde{\boldsymbol{\alpha}}, \widetilde{\theta}, \widetilde{\tau}) = \exp\left\{ \frac{T_s}{N_0} \operatorname{Re}\left[\sum_{k=0}^{NL_0 - 1} x(kT_s)\widetilde{s}^*(kT_s) \right] - \frac{T_s}{2N_0} \sum_{k=0}^{NL_0 - 1} |\widetilde{s}(kT_s)|^2 \right\}, \tag{8}$$

where

$$\widetilde{s}(t) = e^{j\widetilde{\theta}} \sqrt{\frac{2E_s}{T}} e^{j\psi_0(t - \widetilde{\tau}, \widetilde{\boldsymbol{\alpha}}_0)} e^{j\psi_1(t \ \ \widetilde{\tau}, \widetilde{\boldsymbol{\alpha}}_1)}. \tag{9}$$

Since the last sum in equation (8) is independent of $\widetilde{\boldsymbol{\alpha}}$, $\widetilde{\theta}$, and $\widetilde{\tau}$, it suffices to consider

$$\begin{aligned} \Lambda'(\boldsymbol{x}|\widetilde{\boldsymbol{\alpha}}, \widetilde{\theta}, \widetilde{\tau}) &= \exp\left\{ \frac{T_s}{N_0} \operatorname{Re}\left[\sum_{k=0}^{NL_0 - 1} x(kT_s)\widetilde{s}^*(kT_s) \right] \right\} \\ &= \exp\left\{ \frac{T_s}{N_0} \sqrt{\frac{2E_s}{T}} \operatorname{Re}\left[e^{\ j\widetilde{\theta}} \sum_{k=0}^{NL_0 \ \ 1} x(kT_s) \right.\right. \\ &\qquad \left.\left. \times \ e^{\ j\psi_0(kT_s \ \ \widetilde{\tau}, \widetilde{\boldsymbol{\alpha}}_0)} e^{\ j\psi_1(kT_s \ \ \widetilde{\tau}, \widetilde{\boldsymbol{\alpha}}_1)} \right] \right\}. \end{aligned} \tag{10}$$

To obtain practical results, the case of small *signal-to-noise ratio (SNR)* will be considered since a synchronizer that is "optimum" for small SNR should certainly perform well with higher SNR. For small SNR, we have

$$\begin{aligned} \Lambda'(\boldsymbol{x}|\widetilde{\boldsymbol{\alpha}}, \widetilde{\theta}, \widetilde{\tau}) &\cong 1 + \frac{T_s}{N_0} \sqrt{\frac{2E_s}{T}} \operatorname{Re}[Z] \\ &\triangleq \Lambda''(\boldsymbol{x}|\widetilde{\boldsymbol{\alpha}}, \widetilde{\theta}, \widetilde{\tau}), \end{aligned} \tag{11}$$

where

$$Z \triangleq e^{-j\widetilde{\theta}} \sum_{k=0}^{NL_0 \ \ 1} x(kT_s) e^{\ j\psi_0(kT_s \ \ \widetilde{\tau}, \widetilde{\boldsymbol{\alpha}}_0)} e^{\ j\psi_1(kT_s \ \ \widetilde{\tau}, \widetilde{\boldsymbol{\alpha}}_1)}. \tag{12}$$

Averaging over $\widetilde{\boldsymbol{\alpha}}$ in $\Lambda''(\boldsymbol{x}|\widetilde{\boldsymbol{\alpha}}, \widetilde{\theta}, \widetilde{\tau})$, as shown in Appendix A, yields

$$\begin{aligned} \Lambda''(\boldsymbol{x}|\widetilde{\theta}, \widetilde{\tau}) &= 1 + \frac{T_s}{N_0} \sqrt{\frac{2E_s}{T}} E_{\widetilde{\boldsymbol{\alpha}}}\{\operatorname{Re}[Z]\} \\ &= 1 + \frac{T_s}{N_0} \sqrt{\frac{2E_s}{T}} |X| \cos(\phi_X - \widetilde{\theta}), \end{aligned} \tag{13}$$

where

$$X = |X|e^{j\phi_X} = \sum_{k=0}^{NL_0-1} x(kT_s)F(h_0, h_1, kT_s - \tilde{\tau}) \tag{14}$$

and

$$F(h_0, h_1, kT_s - \tilde{\tau}) = \prod_i \cos\left[2\pi h_0 q(kT_s - \tilde{\tau} - 2iT)\right] \cos\left[4\pi h_0 q(kT_s - \tilde{\tau} - 2iT)\right] \times \cos\left[2\pi h_1 q(kT_s - \tilde{\tau} - [2i+1]T)\right] \cos\left[4\pi h_1 q(kT_s - \tilde{\tau} - [2i+1]T)\right]. \tag{15}$$

Note that $F(h_0, h_1, kT_s - \tilde{\tau})$ is real-valued and independent of $\tilde{\theta}$.

Next, we let $\widehat{\theta}_{ML}$ and $\widehat{\tau}_{ML}$ denote the *maximum likelihood estimates* of θ and τ, respectively, *i.e.*, the values of $\tilde{\theta}$ and $\tilde{\tau}$ that maximize $\Lambda''(\boldsymbol{x}|\tilde{\theta}, \tilde{\tau})$. Since $|X|$ is independent of $\tilde{\theta}$, it follows by inspection of equation (13) that $\widehat{\theta}_{ML} = \phi_X$, where ϕ_X is defined as in equation (14). (Technically, $\widehat{\theta}_{ML}$ and $\widehat{\tau}_{ML}$ are only approximations of the ML estimates because of the small SNR approximation above.) Note that $\widehat{\theta}_{ML}$ depends on $\widehat{\tau}_{ML}$, but that the reverse is not true. From equations (13) and (14), it follows that $\widehat{\tau}_{ML}$ is the value of $\tilde{\tau}$ that maximizes $|X|$ or, equivalently, maximizes $|X|^2$, where

$$|X|^2 = \sum_{k_1=0}^{NL_0-1} \sum_{k_2=0}^{NL_0-1} x(k_1T_s)x^*(k_2T_s)F(h_0, h_1, k_1T_s - \tilde{\tau})F(h_0, h_1, k_2T_s - \tilde{\tau}). \tag{16}$$

Since it is mathematically intractable to find $\widehat{\tau}_{ML}$ as a solution either to $\frac{\partial}{\partial\tilde{\tau}}|X| = 0$ or to $\frac{\partial}{\partial\tilde{\tau}}|X|^2 = 0$, we will describe a practical approach to determine an approximate maximum of equation (14) and, thus, an approximate value for $\widehat{\tau}_{ML}$.

We divide the region of uncertainty for $\tilde{\tau}$, namely, the time interval, $T = NT_s$, into N_τ increments, each of width, $\Delta\tilde{\tau}$. Letting m be the number of these increments contained in T_s, it follows that

$$N_\tau = \frac{T}{\Delta\tilde{\tau}} = \frac{NT_s}{\Delta\tilde{\tau}} = Nm. \tag{17}$$

The timing synchronizer may be implemented as shown below (Figure 2) as a group of N *parallel processors*, each of which generates m values of X corresponding to m assumed values of $\tilde{\tau}$. The combination produces a total output of Nm values of X, providing the basis for finding $\widehat{\tau}_{ML}$ and $\widehat{\theta}_{ML}$ by choosing the output with the largest modulus. That is, for each $a = 0, 1, \ldots, Nm-1$, let $\tilde{\tau}_a = a \cdot \Delta\tilde{\tau}$ be the a^{th} *assumed value* of $\tilde{\tau}$ and compute the *corresponding value*, X_a, by substituting $\tilde{\tau}_a$ into equation (14). Next, determine the value $a_0 \in \{0, 1, \ldots Nm-1\}$ such that

$$|X_{a_0}| = \max\{|X_a| : a = 0, 1, \ldots, Nm-1\}.$$

Finally, it follows that

$$\widehat{\tau}_{ML} \cong \tilde{\tau}_{a_0} = a_0 \cdot \Delta\tilde{\tau} \tag{18}$$

and, since $X_{a_0} = |X_{a_0}|\exp(j\phi_{X_{a_0}})$, it also follows that

$$\widehat{\theta}_{ML} \cong \phi_{X_{a_0}}. \tag{19}$$

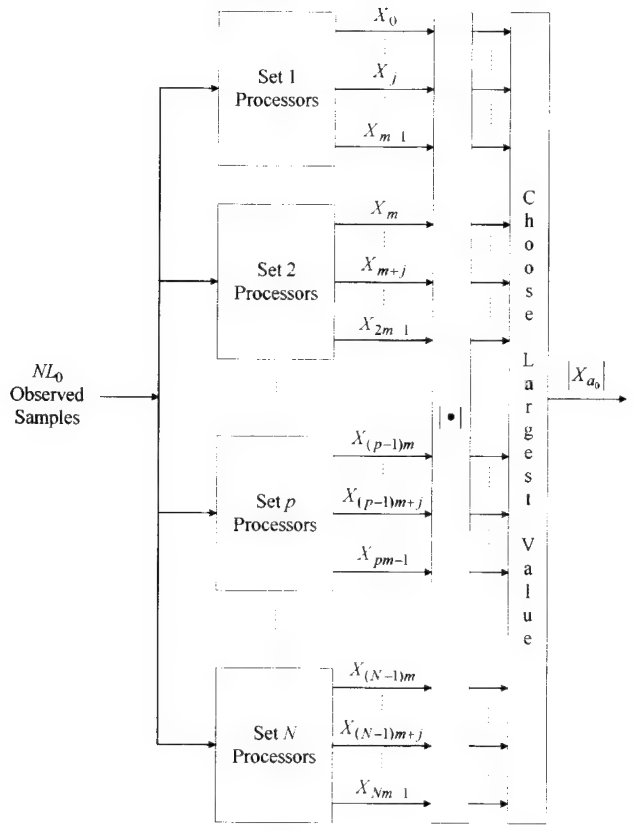

Fig. 2. Parallel processors.

Computation of $X_{(p-1)m+j}$, the j^{th} output of the p^{th} processor (Figure 2), for $p = 1, 2, \ldots, N$ and $j = 0, 1, 2, \ldots, m-1$, as derived in Appendix B, is performed according to the block diagram (Figure 3), in which the scalars, $K_0(h_0)$ and $K_1(h_1)$, are defined as

$$K_0(h_0) = \cos(\pi h_0)\cos(2\pi h_0) \tag{20}$$

and

$$K_1(h_1) = \cos(\pi h_1)\cos(2\pi h_1), \tag{21}$$

and the $N \times 1$ column vectors, $\mathbf{V_0}(h_0, m, j)$ and $\mathbf{V_1}(h_1, m, j)$, are given by

$$\mathbf{V_0}(h_0, m, j) = \begin{bmatrix} \cos\left[(\pi h_0/N)\,(1 - j/m)\right]\cos\left[(2\pi h_0/N)\,(1 - j/m)\right] \\ \cos\left[(\pi h_0/N)\,(2 - j/m)\right]\cos\left[(2\pi h_0/N)\,(2 - j/m)\right] \\ \vdots \\ \cos\left[(\pi h_0/N)\,(N - j/m)\right]\cos\left[(2\pi h_0/N)\,(N - j/m)\right] \end{bmatrix} \tag{22}$$

and

$$\mathbf{V_1}(h_1, m, j) = \begin{bmatrix} \cos\left[(\pi h_1/N)\,(N + 1 - j/m)\right]\cos\left[(2\pi h_1/N)\,(N + 1 - j/m)\right] \\ \cos\left[(\pi h_1/N)\,(N + 2 - j/m)\right]\cos\left[(2\pi h_1/N)\,(N + 2 - j/m)\right] \\ \vdots \\ \cos\left[(\pi h_1/N)\,(2N - j/m)\right]\cos\left[(2\pi h_1/N)\,(2N - j/m)\right] \end{bmatrix}. \tag{23}$$

The $1 \times N$ input row vectors, $\mathbf{x}_{lN}^{(p)}$, are defined by

$$\mathbf{x}_{lN}^{(p)} = \left[x\left([p + (l-1)N]\,T_s\right), x\left([p + (l-1)N + 1]\,T_s\right), \ldots, x\left([p - 1 + lN]\,T_s\right)\right], \tag{24}$$

for $l = 1, 2, \ldots, L_0$; for those values of indices greater than $NL_0 - 1$, the upper limit for the actual samples given in equation (7), we set

$$x(L_0 N T_s) = x([L_0 N + 1]T_s) = \cdots = x([L_0 N + p - 1]T_s) = 0. \tag{25}$$

For each fixed value of p, m different values, $\{X_{(p\ \ 1)m+j} : j = 0, 1, 2, \ldots, m-1\}$, are generated corresponding to the m different values of the vector pair, $\mathbf{V_0}(h_0, m, j)$ and $\mathbf{V_1}(h_1, m, j)$. As p varies, the input row vectors change as does the input to the final summation producing $X_{(p\_1)m+j}$.

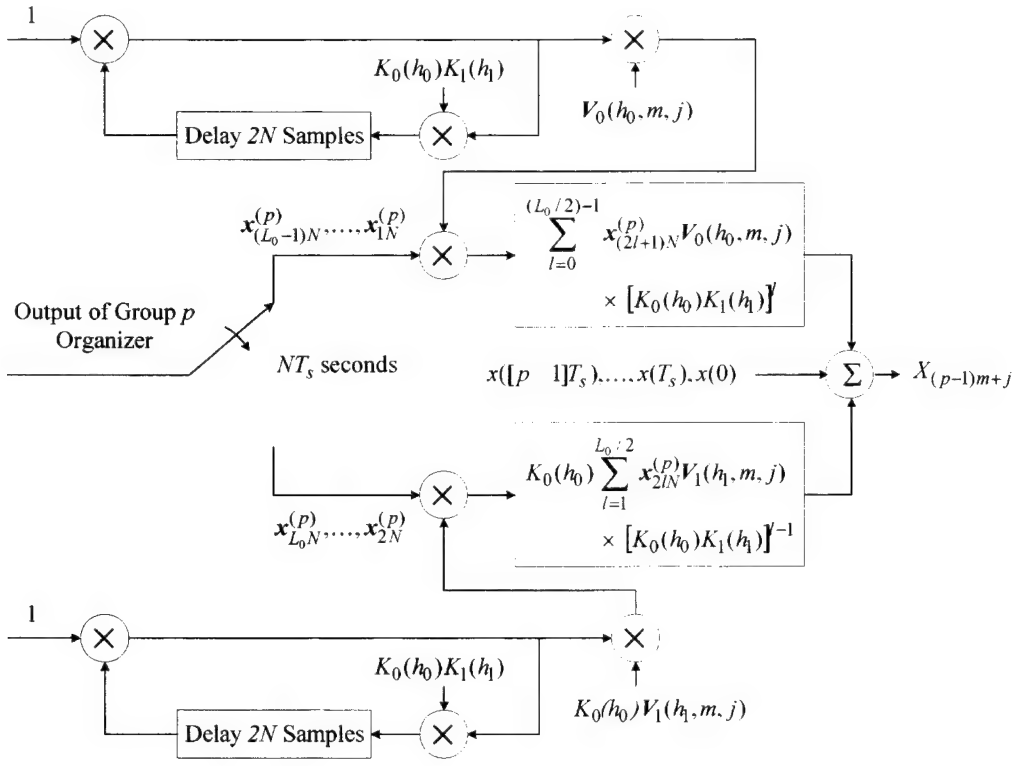

Fig. 3. Calculation of $X_{(p\_1)m+j}$ by the p^{th} parallel processor, for $p = 1, 2, \ldots, N$ and $j = 0, 1, \ldots, m\ \ 1$.

Summarizing, the calculation of $X_{(p\ \ 1)m+j}$, and thus of $\widehat{\tau}_{ML}$ and $\widehat{\theta}_{ML}$, is performed as described in the following algorithm.

Step 1: Pass the received signal, $r(t)$, through the AAF, and sample the resulting band-limited waveform (Figure 1).

Step 2: Collect and organize the NL_0 samples into N groups (each group includes all NL_0 samples) for input into N sets of parallel processors as described below.

Group 1: $x(0), \mathbf{x}^{(1)}_{1N}, \mathbf{x}^{(1)}_{2N}, \ldots, \mathbf{x}^{(1)}_{L_0N}$.

Group 2: $x(0), x(T_s), \mathbf{x}^{(2)}_{1N}, \mathbf{x}^{(2)}_{2N}, \ldots, \mathbf{x}^{(2)}_{L_0N}$.

$\vdots$

Group p: $x(0), x(T_s), x(2T_s), \ldots, x([p\ \_\ 1]T_s), \mathbf{x}^{(p)}_{1N}, \mathbf{x}^{(p)}_{2N}, \ldots, \mathbf{x}^{(p)}_{L_0N}$.

$\vdots$

Group N: $x(0), x(T_s), x(2T_s), \ldots, x([N\ \_\ 1]T_s), \mathbf{x}^{(N)}_{1N}, \mathbf{x}^{(N)}_{2N}, \ldots, \mathbf{x}^{(N)}_{L_0N}$.

Step 3: Calculate the Nm values of X, using N parallel sets of processors. For example, the p^{th} set of processors associated with Group p input above, produces the m values, $\{X_{(p\ \ 1)m+j} : j = 0, 1, 2, \ldots, m-1\}$.

Step 4: Compute $\{|X_{(p\ \ 1)m+j}|^2 : p = 1, 2, \ldots, N;\ j = 0, 1, 2, \ldots, m-1\}$ and choose the largest value, say $|X_{a_0}|^2$, where $X_{a_0} = |X_{a_0}| \exp(j\phi_{X_{a_0}})$.

Step 5: Compute $\widehat{\tau}_{ML}$ and $\widehat{\theta}_{ML}$, as in equations (18) and (19), respectively.

III. Compact Description of Phase and Timing Synchronizer

From the NL_0 samples, $x(0), x(T_s), \ldots, x([NL_0 \quad 1]T_s)$, form the row vectors $\mathbf{x}_{lN}^{(p)}$ previously defined in equation (24) for $p = 1, 2, \ldots, N$ and $l = 1, 2, \ldots, L_0$. We note from equations (24) and (25), when $l = L_0$ and $p = N$, then

$$\mathbf{x}_{L_0N}^{(N)} = [0, 0, \ldots, 0], \tag{26}$$

and we extend the definition of $\mathbf{x}_{lN}^{(p)}$ to the case when $l = 0$ and $p = 1$ by defining the vector

$$\mathbf{x}_{0N}^{(1)} = [x(0), x(T_s), \ldots, x([N \quad 1]T_s)]\,. \tag{27}$$

We also define the $1 \times N$ row vector

$$\mathbf{P}^{(p)} = [\underbrace{1, 1, \ldots, 1}_{p}, \underbrace{0, 0, \ldots 0}_{N \quad p}] \tag{28}$$

and the $1 \times L_0/2$ row vector

$$\mathbf{K}_0 = \left[1, K_0(h_0)K_1(h_1), \{K_0(h_0)K_1(h_1)\}^2, \ldots, \{K_0(h_0)K_1(h_1)\}^{\frac{L_0}{2} \quad 1}\right], \tag{29}$$

where $K_0(h_0)$, $K_1(h_1)$ are as defined previously in equations (20) and (21), respectively. Then, we define the $N \times m$ matrices

$$\mathbf{V}^{(0)} = [\mathbf{V}_0(h_0, m, 0), \mathbf{V}_0(h_0, m, 1), \ldots, \mathbf{V}_0(h_0, m, m-1)] \tag{30}$$

and

$$\mathbf{V}^{(1)} = [\mathbf{V}_1(h_1, m, 0), \mathbf{V}_1(h_1, m, 1), \ldots, \mathbf{V}_1(h_1, m, m-1)]\,, \tag{31}$$

where $\mathbf{V}_0(h_0, m, j)$ and $\mathbf{V}_1(h_1, m, j)$ were defined previously in equations (22) and (23), respectively. Next, letting $\mathbf{A}^T$ denote the transpose of $\mathbf{A}$, we define three other matrices that are each functions of the NL_0 samples: the $N \times m$ matrix,

$$\mathbf{x}_{0N} = \left[\underbrace{\left(\mathbf{x}_{0N}^{(1)}\right)^T, \left(\mathbf{x}_{0N}^{(1)}\right)^T, \ldots, \left(\mathbf{x}_{0N}^{(1)}\right)^T}_{m}\right], \tag{32}$$

and the $L_0/2 \times N$ matrices,

$$\mathbf{x}_{odd}^{(p)} = \begin{bmatrix} \mathbf{x}_{lN}^{(p)} \\ \mathbf{x}_{3N}^{(p)} \\ \vdots \\ \mathbf{x}_{(L_0 \quad 1)N}^{(p)} \end{bmatrix} \tag{33}$$

and

$$\mathbf{x}_{even}^{(p)} = \begin{bmatrix} \mathbf{x}_{2N}^{(p)} \\ \mathbf{x}_{4N}^{(p)} \\ \vdots \\ \mathbf{x}_{L_0N}^{(p)} \end{bmatrix}. \tag{34}$$

Finally, using the vectors and matrices just defined, the calculation of the Nm values of X, namely $X_0, X_1, \ldots, X_{Nm \quad 1}$, can be represented in compact form in terms of matrix operations. As shown in the block diagram (Figure 3), a general value of X, say $X_{(p \quad 1)m+j}$, is computed as the grand total of two summation expressions in the upper and lower portion of the diagram and a sum of sample values in the middle. For a fixed value of p and with j varying between 0 and $m \_ 1$, it can be readily shown that $\mathbf{K}_0\mathbf{x}_{odd}^{(p)}\mathbf{V}^{(0)}$ and $K_0(h_0)\mathbf{K}_0\mathbf{x}_{even}^{(p)}\mathbf{V}^{(1)}$ represent the values of the summation expressions in the upper and lower portions of the block diagram, respectively, and that $\mathbf{P}^{(p)}\mathbf{x}_{0N}$ represents the sum of sample values in the middle. Hence, all Nm values of X can be calculated as

$$\left[X_{(p\_1)m}, X_{(p\_1)m+1}, \ldots, X_{(p\_1)m+j}, \ldots, X_{pm\_1}\right] = \mathbf{P}^{(p)}\mathbf{x}_{0N} + \mathbf{K}_0\mathbf{x}_{odd}^{(p)}\mathbf{V}^{(0)} + K_0(h_0)\mathbf{K}_0\mathbf{x}_{even}^{(p)}\mathbf{V}^{(1)}, \tag{35}$$

for $p = 1, 2, \ldots, N$.

This Page Intentionaly
Left Blank

IV. Conclusions

This document presents the derivation of a joint phase and timing synchronizer, assuming frequency is known, for dual-h, full-response, 4-ary CPM with 1REC instantaneous frequency pulse. The synchronizer is based upon the maximum-likelihood criterion, with the final structure resulting from certain approximations made to overcome various mathematical complexities and to make any subsequent implementation of reasonable complexity.

It is not clear that this new synchronizer provides significant, if any, benefits compared with others in use or proposed for specific applications. Comparisons based upon simulation are required before any further conclusions can be made.

V. REFERENCES

[1] U. Mengali and A. N. D'Andrea. 1997. *Synchronization Techniques for Digital Receivers*. Plenum Press, New York, NY.

[2] J. B. Anderson, T. Aulin, and C.-E. Sundberg. 1986. *Digital Phase Modulation*. Plenum Press, New York, NY.

[3] R. H. Pettit and B. E. Wahlen. 2000. "A maximum-likelihood-based frequency synchronizer for dual-h full-response 4-ary continuous-phase modulation (CPM)," TD 3094 (Feb). SSC San Diego, CA.

[4] H. L. Van Trees. 1968. *Detection, Estimation, and Modulation: Part I*. Wiley, New York, NY.

APPENDIX A
CONDITIONAL LIKELIHOOD FUNCTION AVERAGED OVER RANDOM DATA SYMBOLS

The conditional likelihood, $\Lambda''(\boldsymbol{x}|\widetilde{\theta},\widetilde{\tau})$, given in equation (13), is obtained by averaging $\mathrm{Re}[Z]$ over $\widetilde{\boldsymbol{\alpha}}$, with Z given in equation (12). Since the data symbols occur independently, we consider separately the two averages,

$$E_{\boldsymbol{\alpha}_0}\left\{\exp\left[-j\psi_0(kT_s-\widetilde{\tau},\widetilde{\boldsymbol{\alpha}}_0)\right]\right\}$$

and

$$E_{\boldsymbol{\alpha}_1}\left\{\exp\left[-j\psi_1(kT_s-\widetilde{\tau},\widetilde{\boldsymbol{\alpha}}_1)\right]\right\}.$$

Consider the first term:

$$\begin{aligned}
E_{\boldsymbol{\alpha}_0}\left\{\exp\left[-j\psi_0(kT_s-\widetilde{\tau},\widetilde{\boldsymbol{\alpha}}_0)\right]\right\} &= E_{\widetilde{\boldsymbol{\alpha}}_0}\left\{\exp\left[\;j2\pi h_0\sum_i\widetilde{\alpha}_{2i}q(kT_s\;\;\widetilde{\tau}\;\;2iT)\right]\right\}\\
&= E_{\widetilde{\boldsymbol{\alpha}}_0}\left\{\prod_i\exp\left[\;j2\pi h_0\widetilde{\alpha}_{2i}q(kT_s\;\;\widetilde{\tau}\;\;2iT)\right]\right\}\\
&= \prod_i E_{\alpha_{2i}}\left\{\exp\left[-j2\pi h_0\widetilde{\alpha}_{2i}q(kT_s-\widetilde{\tau}-2iT)\right]\right\}\\
&= \prod_i(1/4)\left\{\exp\left[j6\pi h_0q(kT_s-\widetilde{\tau}-2iT)\right]+\exp\left[-j6\pi h_0q(kT_s-\widetilde{\tau}-2iT)\right]\right.\\
&\quad\left.+\exp\left[j2\pi h_0q(kT_s-\widetilde{\tau}-2iT)\right]+\exp\left[-j2\pi h_0q(kT_s-\widetilde{\tau}-2iT)\right]\right\}\\
&= \prod_i(1/2)\left\{\cos\left[6\pi h_0q(kT_s-\widetilde{\tau}-2iT)\right]+\cos\left[2\pi h_0q(kT_s-\widetilde{\tau}-2iT)\right]\right\}.
\end{aligned}$$

Similarly,

$$\begin{aligned}
E_{\boldsymbol{\alpha}_1}\left\{\exp\left[-j\psi_1(kT_s-\widetilde{\tau},\widetilde{\boldsymbol{\alpha}}_1)\right]\right\} &= \prod_i(1/2)\left\{\cos\left[6\pi h_1q(kT_s-\widetilde{\tau}-[2i+1]T)\right]\right.\\
&\quad\left.+\cos\left[2\pi h_1q(kT_s-\widetilde{\tau}-[2i+1]T)\right]\right\}.
\end{aligned}$$

Using the identity, $\cos 3\beta+\cos\beta=2\cos\beta\cos 2\beta$, yields the result in equation (13).

APPENDIX B
CALCULATION OF $X_{(p\ \ 1)m+j}$

In this appendix we derive the mathematical expression for $X_{(p\ \ 1)+j}$, the output of the parallel processor in the general case (Figure 3). Based on the definition of $\widetilde{\tau}_a$ (section II) and equation (14), it follows that

$$X_{(p\_1)m+j} = \sum_{k=0}^{NL_0\_1} x(kT_s)F(h_0, h_1, kT_s \quad \widetilde{\tau}_a),$$

where $\widetilde{\tau}_a = a \cdot \Delta\widetilde{\tau}$ and $a = (p-1)m+j$, $p = 1, 2, \ldots, N$, and $j = 0, 1, \ldots, m-1$. Expanding the above summation into several sums yields

$$\begin{aligned} X_{(p\ \ 1)m+j} &= \sum_{k=0}^{p\ \ 1} x(kT_s)F(h_0, h_1, kT_s - \widetilde{\tau}_a) + \sum_{k=p}^{(p\ \ 1)+N} x(kT_s)F(h_0, h_1, kT_s - \widetilde{\tau}_a) + \ldots \\ &\quad \ldots + \sum_{k=p+(r\ \ 1)N}^{(p\_1)+rN} x(kT_s)F(h_0, h_1, kT_s - \widetilde{\tau}_a) + \ldots + \sum_{k=p+(L_0\ \ 1)N}^{(p\ \ 1)+L_0N} x(kT_s)F(h_0, h_1, kT_s - \widetilde{\tau}_a) \\ &= \sum_{k=0}^{p\ \ 1} x(kT_s)F(h_0, h_1, kT_s - \widetilde{\tau}_a) + \sum_{r=1}^{L_0} \sum_{k=p+(r\ \ 1)N}^{(p\ \ 1)+rN} x(kT_s)F(h_0, h_1, kT_s - \widetilde{\tau}_a), \end{aligned} \tag{B.1}$$

where $F(h_0, h_1, kT_s - \widetilde{\tau}_a)$ is the product defined in equation (15) with indices $i = 0, 1, \ldots, L_0/2 - 1$. (We remark that the last $p-1$ values of $x(kT_s)$ in the second summation in the last line of equation (B.1) are 0, as noted in equation (25) above.)

The function $F(h_0, h_1, kT_s \_ \widetilde{\tau})$ is very complicated, having $L_0/2$ sets of four cosine factors and exhibiting a complex interaction between the summation index k of equation (14) and the product index i of equation (15). The calculation of each $X_{(p\_1)m+j}$ requires repeated calculation of $F(h_0, h_1, kT_s \quad \widetilde{\tau}_a)$, which can be broken down into four cases, depending on the values of $\widetilde{\tau}_a$, k, and i as described below.

Case 1: $(k \_ 2Ni)T_s \le \widetilde{\tau}_a$

$$\begin{aligned} \cos[2\pi h_0 q(kT_s - \widetilde{\tau}_a - 2iT)] &= \cos[4\pi h_0 q(kT_s - \widetilde{\tau}_a - 2iT)] = 1 \\ \cos[2\pi h_1 q(kT_s - \widetilde{\tau}_a - [2i+1]T)] &= \cos[4\pi h_1 q(kT_s - \widetilde{\tau}_a - [2i+1]T)] = 1 \end{aligned}$$

Case 2: $\widetilde{\tau}_a < (k - 2Ni)T_s \le T + \widetilde{\tau}_a$

$$\begin{aligned} \cos[2\pi h_0 q(kT_s - \widetilde{\tau}_a - 2iT)] &= \cos[2\pi h_0\{(k/2N) - i - (\widetilde{\tau}_a/2NT_s)\}] \\ \cos[4\pi h_0 q(kT_s - \widetilde{\tau}_a - 2iT)] &= \cos[4\pi h_0\{(k/2N) - i - (\widetilde{\tau}_a/2NT_s\}] \\ \cos[2\pi h_1 q(kT_s - \widetilde{\tau}_a - [2i+1]T)] &= \cos[4\pi h_1 q(kT_s - \widetilde{\tau}_a - [2i+1]T)] = 1 \end{aligned}$$

Case 3: $T + \widetilde{\tau}_a < (k - 2Ni)T_s \le 2T + \widetilde{\tau}_a$

$$\begin{aligned} \cos[2\pi h_0 q(kT_s - \widetilde{\tau}_a - 2iT)] &= \cos \pi h_0 \\ \cos[4\pi h_0 q(kT_s - \widetilde{\tau}_a - 2iT)] &= \cos 2\pi h_0 \\ \cos[2\pi h_1 q(kT_s - \widetilde{\tau}_a - [2i+1]T)] &= \cos[2\pi h_1\{(k/2N) - i - (\widetilde{\tau}_a/2NT_s)\}] \\ \cos[4\pi h_1 q(kT_s - \widetilde{\tau}_a - [2i+1]T)] &= \cos[4\pi h_1\{(k/2N) - i - (\widetilde{\tau}_a/2NT_s)\}] \end{aligned}$$

Case 4: $(k - 2Ni)T_s > 2T + \widetilde{\tau}_a$

$$\begin{aligned} \cos[2\pi h_0 q(kT_s - \widetilde{\tau}_a - 2iT)] &= \cos \pi h_0 \\ \cos[4\pi h_0 q(kT_s - \widetilde{\tau}_a - 2iT)] &= \cos 2\pi h_0 \\ \cos[2\pi h_1 q(kT_s - \widetilde{\tau}_a - [2i+1]T)] &= \cos \pi h_1 \\ \cos[4\pi h_1 q(kT_s - \widetilde{\tau}_a - [2i+1]T)] &= \cos 2\pi h_1 \end{aligned}$$

Determining which of the four cases applies for a particular (i, k) pair is greatly facilitated by drawing in the (i, k)-plane (Figure 4) the boundaries $k = 2Ni$, $k = (2i + 1)N$, and $k = (2i + 2)N$, which apply for $\tilde{\tau} = 0$, and then inferring the effects of $\tilde{\tau} \neq 0$ on the choice of factors.

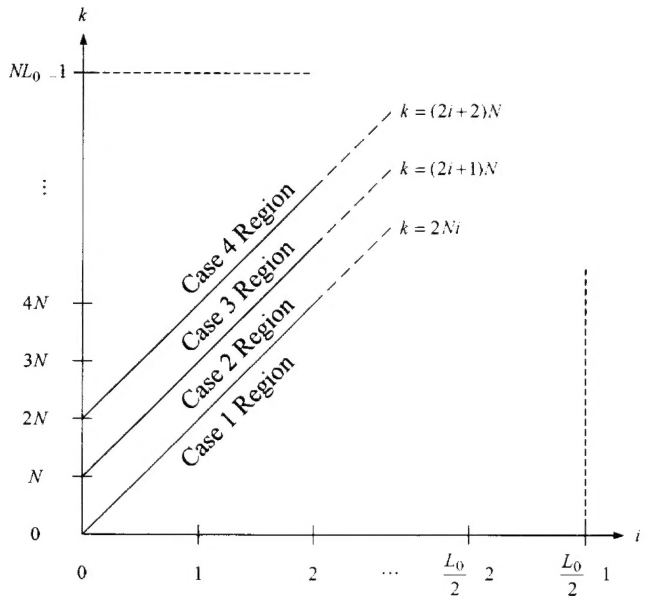

Fig. 4. Regions for factors of $F(h_0, h_1, kT_s \quad \tilde{\tau})$.

For $k = 0, 1, \ldots, p \_ 1$ and $i = 0, 1, \ldots, L_0/2 \quad 1$, it follows that

$$\begin{aligned}
(k _ 2Ni)T_s &= (k \quad 2Ni)m \cdot \Delta\tilde{\tau} \\
&\leq [(p-1) - 2Ni]\, m \cdot \Delta\tilde{\tau} \\
&= [(p-1)m - 2Nim] \cdot \Delta\tilde{\tau} \\
&\leq [(p-1)m + j] \cdot \Delta\tilde{\tau} \\
&= a \cdot \Delta\tilde{\tau} \\
&= \tilde{\tau}_a,
\end{aligned}$$

where the first equality holds by the definition of T_s in equation (17), the first inequality holds since $0 \leq k \leq p - 1$, and the second inequality holds since $2Nim \geq 0$ and $j \geq 0$. Thus, Case 1 holds for all values of k in the first sum in equation (B.1) above, which implies that $F(h_0, h_1, kT_s - \tilde{\tau}_a) \equiv 1$ for such k and that, therefore, this sum is equal to $\sum_{k=0}^{p-1} x(kT_s)$. Hence, it follows that

$$X_{(p \_ 1)m+j} = \sum_{k=0}^{p \_ 1} x(kT_s) + \sum_{r=1}^{L_0} \sum_{k=p+(r \quad 1)N}^{(p \_ 1)+rN} x(kT_s) F(h_0, h_1, kT_s \_ \tilde{\tau}_a),$$

which can be expanded as

$$X_{(p \quad 1)m+j} = \sum_{k=0}^{p \quad 1} x(kT_s) + \sum_{\substack{r=1 \\ r \text{ odd}}}^{L_0} \sum_{k=p+(r \_ 1)N}^{(p \quad 1)+rN} x(kT_s) F(h_0, h_1, kT_s \_ \tilde{\tau}_a) + \sum_{\substack{r=1 \\ r \text{ even}}}^{L_0} \sum_{k=p+(r \_ 1)N}^{(p \quad 1)+rN} x(kT_s) F(h_0, h_1, kT_s \_ \tilde{\tau}_a).$$

Noting that the odd values of r between 1 and L_0 may be expressed as $r = 2l + 1$, for $l = 0, 1, \ldots, L_0/2 \_ 1$, and the even values of r may be expressed as $r = 2l$, for $l = 1, 2, \ldots, L_0/2$, we observe that the last equation for $X_{(p \_ 1)m+j}$

may be written equivalently as

$$X_{(p-1)m+j} = \sum_{k=0}^{p-1} x(kT_s) + \sum_{l=0}^{(L_0/2)-1} \sum_{k=p+2lN}^{(p-1)+(2l+1)N} x(kT_s)F(h_0, h_1, kT_s - \tilde{\tau}_a) + \sum_{l=1}^{L_0/2} \sum_{k=p+(2l-1)N}^{(p-1)+2lN} x(kT_s)F(h_0, h_1, kT_s - \tilde{\tau}_a). \quad \text{(B.2)}$$

To verify the calculation of $X_{(p-1)m+j}$ depicted in the block diagram above (Figure 3), we observe that the value of the first sum in equation (B.2) equals the sum of sample values, $x([p-1]T_s), \ldots, x(T_s), x(0)$, entering the summation operator in the middle of the figure. We claim further that the values of the second and third sums in equation (B.2) equal the values output by the upper and lower blocks, respectively, which enter the summation operation in the figure. We now prove these claims.

To evaluate the two double sums in equation (B.2), the interaction between the summation index, k, of the inner sums and the product index, i, of equation (15) must be understood. After some analysis, the combinations of k and i belonging to each of the four cases described above can be determined as tabulated (Table I). Using the results for $k = p + 2lN + b$ to evaluate $F(h_0, h_1, kT_s - \tilde{\tau}_a)$, substituting $[(p-1)m + j]T_s/m$ for $\tilde{\tau}_a$, and making an obvious change of summation index yields that

$$\begin{aligned} \sum_{k=p+2lN}^{(p-1)+(2l+1)N} x(kT_s)F(h_0, h_1, kT_s - \tilde{\tau}_a) &= [K_0(h_0)K_1(h_1)]^l \sum_{b=0}^{N-1} x([p + 2lN + b]T_s) \\ &\quad \times \cos[(\pi h_0/N)(1 + b - j/m)] \\ &\quad \times \cos[(2\pi h_0/N)(1 + b - j/m)] \\ &= [K_0(h_0)K_1(h_1)]^l \mathbf{x}^{(p)}_{(2l+1)N} \mathbf{V}_0(h_0, m, j), \end{aligned} \quad \text{(B.3)}$$

where $K_0(h_0)$, $K_1(h_1)$, $\mathbf{x}^{(p)}_{(2l+1)N}$ and $\mathbf{V}_0(h_0, m, j)$ are as defined in equations (20), (21), (24), and (22), respectively. Similarly, using the results for $k = p + (2l-1)N + b$, it can be shown that

$$\begin{aligned} \sum_{k=p+(2l-1)N}^{(p-1)+2lN} x(kT_s)F(h_0, h_1, kT_s - \tilde{\tau}_a) &= K_0(h_0)[K_0(h_0)K_1(h_1)]^{l-1} \sum_{b=0}^{N-1} x([p + (2l-1)N + b]T_s) \\ &\quad \times \cos[(\pi h_1/N)(N + 1 + b - j/m)] \\ &\quad \times \cos[(2\pi h_1/N)(N + 1 + b - j/m)] \\ &= K_0(h_0)[K_0(h_0)K_1(h_1)]^{l-1} \mathbf{x}^{(p)}_{2lN} \mathbf{V}_1(h_1, m, j), \end{aligned} \quad \text{(B.4)}$$

where $\mathbf{x}^{(p)}_{2lN}$ and $\mathbf{V}_1(h_1, m, j)$ are as defined in equations (24) and (23), respectively. Substitution of equations (B.3) and (B.4) into equation (B.2) proves the two claims above, which completes the derivation of $X_{(p-1)m+j}$.

TABLE I

Values of i satisfying cases 1, 2, 3, and 4, for given values of k ($b = 0, 1, \ldots, N-1$).

		Values of i Satisfying:			
l	k	Case 1	Case 2	Case 3	Case 4
$0, 1, \ldots, (L_0/2)-1$	$p + 2lN + b$	$l+1, l+2, \ldots, (L_0/2)-1$	l	None	$0, 1, \ldots, l-1$
$1, 2, \ldots, L_0/2$	$p + (2l-1)N + b$	$l, l+1, \ldots, L_0/2$	None	$l-1$	$0, 1, \ldots, l-2$

REPORT DOCUMENTATION PAGE

Form Approved
OMB No. 0704-01-0188

PLEASE DO NOT RETURN YOUR FORM TO THE ABOVE ADDRESS.

1. REPORT DATE *(DD-MM-YYYY)*	2. REPORT TYPE	3. DATES COVERED *(From - To)*
09–2002	Technical	

4. TITLE AND SUBTITLE
A JOINT MAXIMUM-LIKELIHOOD-BASED PHASE AND TIMING SYNCHRONIZER FOR DUAL-*h*, FULL-RESPONSE 4-ARY CPM

5a. CONTRACT NUMBER

5b. GRANT NUMBER

5c. PROGRAM ELEMENT NUMBER

6. AUTHORS
R. H. Pettit
California State University, Northridge

B. E. Wahlen
SSC San Diego

5d. PROJECT NUMBER
0601152N

5e. TASK NUMBER

5f. WORK UNIT NUMBER

7. PERFORMING ORGANIZATION NAME(S) AND ADDRESS(ES)
SSC San Diego
San Diego, CA 92152–5001

8. PERFORMING ORGANIZATION REPORT NUMBER
TD 3143

9. SPONSORING/MONITORING AGENCY NAME(S) AND ADDRESS(ES)
Office of Naval Research, Code 32US
800 North Quincy Street
Arlington, VA 22217–5660

10. SPONSOR/MONITOR'S ACRONYM(S)
ONR

11. SPONSOR/MONITOR'S REPORT NUMBER(S)

12. DISTRIBUTION/AVAILABILITY STATEMENT
Approved for public release; distribution is unlimited.

13. SUPPLEMENTARY NOTES

14. ABSTRACT
Maximum likelihood techniques are useful in finding synchronizer structures for various cases. Synchronizers for frequency, phase, and timing have been found for various bandpass signaling techniques such as PSK, DPSK, QAM, MSK, and CPM. These include data-aided, decision-directed, and clock-aided cases. This report describes a new non-data-aided, non-decision-directed ML-based phase and timing synchronizer for a dual-*h*, full-response, 4-ary CPM waveform. The derived structure will be incorporated into future simulations to compare performance among several possible phase and timing synchronizations.

15. SUBJECT TERMS
Mission Area: Command, Control, and Communications
dual-*h* continuous phase modulation (CPM)
maximum-likelihood

16. SECURITY CLASSIFICATION OF:			17. LIMITATION OF ABSTRACT	18. NUMBER OF PAGES	19a. NAME OF RESPONSIBLE PERSON
a. REPORT	b. ABSTRACT	c. THIS PAGE			B. E. Wahlen
U	U	U	UU	34	19B. TELEPHONE NUMBER *(Include area code)* (619) 553–5622

INITIAL DISTRIBUTION

20012	Patent Counsel	(1)
202753	Archive/Stock	(1)
202752	Library	(1)
2027	M. E. Cathcart	(1)
20275	E. R. Ratliff	(1)
202753	D. Richter	(1)
2846	B. E. Wahlen	(25)

Defense Technical Information Center
Fort Belvoir, VA 22060–6218 (4)

SSC San Diego Liaison Office
C/O PEO-SCS
Arlington, VA 22202–4804

Center for Naval Analyses
Alexandria, VA 22311–1850

Office of Naval Research
ATTN: NARDIC (Code 362)
Arlington, VA 22217–5660

Government-Industry Data Exchange
Program Operations Center
Corona, CA 91718–8000